Pergamon

0734-743X(94)00049-2

Int. J. Impact Engng Vol. 16, No. 3, pp. 375–395, 1995
Elsevier Science Ltd
Printed in Great Britain
0734–743X/95 $9.50 + 0.00

DEVELOPMENT OF SHEAR BANDS IN DYNAMIC PLANE STRAIN COMPRESSION OF DEPLETED URANIUM AND TUNGSTEN BLOCKS

R. C. BATRA† and Z. PENG‡

†Department of Engineering Science & Mechanics, Virginia Polytechnic Institute and State University, Blacksburg, VA 24061-0219 and ‡27124 Yorkshire Sq. #108 Dearborn Heights, MI 48127, U.S.A.

(*Received* 20 *May* 1994; *in revised form* 21 *September* 1994)

Summary—We study the initiation and growth of shear bands in prismatic bodies of rectangular cross-section made of either depleted uranium or tungsten and deformed in plane strain compression at a nominal strain-rate of $5000\,s^{-1}$. It is assumed that defects are distributed symmetrically with respect to the two centroidal axes and each quadrant has up to 300 randomly distributed defects in the form of a weaker material; the flow stress for the weaker material in a quasistatic simple compression test is taken to be 5% lower than that for the original material. It is found that, in the deformed configuration, shear bands in depleted uranium blocks are inclined at approximately 42.5° counterclockwise from the horizontal axis, those in tungsten are inclined at nearly 135°. When shear bands initiate, the total compressive force required to deform the body drops sharply for the uranium blocks but gradually for the tungsten blocks. After a shear band has developed, dead zones form in both uranium and tungsten blocks; the size of the dead zone in the tungsten block is more than that in the uranium block. When the shear modulus for the tungsten is artificially changed so as to equal that for the uranium, the angle of inclination for the shear bands in tungsten blocks changes to that found for the uranium blocks. This suggests that the value of the shear modulus plays a noticeable role in the development of shear bands. We have also studied the effect, on the initiation of shear band, of modeling the defects as either very weak or very strong material.

INTRODUCTION

Magness and Farrand [1] have recently pointed out that when identical cylindrical rods of depleted uranium and tungsten impact steel plates at normal incidence, depleted uranium rods penetrate deeper than the tungsten rods. They explained this difference by suggesting that shear bands near the penetrator nose develop sooner in depleted uranium than in tungsten, leading to the earlier failure and thus pointed-nose shape for depleted uranium penetrators. Batra *et al.* [2] studied torsional deformations of thin tubular specimens, identical to those used by Marchand and Duffy [3], made of twelve different materials and twisted at a nominal strain rate of $5000\,s^{-1}$. They found that shear bands initiated, as indicated by a sharp drop in the torque required to deform the tube, sooner in tungsten than in uranium. In each case the dependence of the material's flow strength upon the effective plastic strain, effective plastic strain rate and temperature was modeled by the Johnson–Cook relation [4] and values of material parameters were taken from Rajendran's [5] report. Of course, the stress-state at points close to the penetrator nose surface is quite different from that of simple shear. This motivated us to study the initiation and development of adiabatic shear bands in uranium and tungsten blocks deformed in plane strain compression.

Backmann and Finnegan [6], amongst others, have pointed out that shear bands initiate from a material defect or inhomogeneity in the body. Nearly all of the previous studies (e.g. see the species issues of *Applied Mechanics Reviews* [7], and the *Mechanics of Materials Journal* [8]) have assumed one or at most two defects in the body located at predetermined positions. Here we assume that the cross-section of the body is rectangular, deformations are symmetrical about the horizontal and vertical centroidal axes, the quarter of the cross-section is divided into 10^4 uniform rectangular elements, and there are up to 300

randomly distributed defects, each modeled as a weak element, in the quarter of the cross-section. The presumed symmetry of deformations requires that defects be distributed symmetrically about the two centroidal axes. The flow stress in a quasistatic simple compression test of these weak elements is taken to be 5% lower than that of the original material. It is found that two or more shear bands form in uranium and tungsten blocks, the effective plastic strain within these bands need not be the same and the one with the most effective plastic strain is inclined at nearly 42.5° counterclockwise with the horizontal axis for the uranium block and 135° for the tungsten block. If the noticeable drop in the compressive load required to deform the material is taken as the criterion for the initiation of shear bands, then shear bands initiate sooner in tungsten than in uranium. This ranking agrees with that found in torsional tests conducted by Johnson *et al.* [4] and also computed by Batra *et al.* [2] in specimens deformed in torsion, but is opposite to that conjectured by Magness and Farrand [1]. The effects of having 100 or 200 randomly distributed weak elements and modeling the defects as either essentially voids or as rigid inclusions have also been scrutinized.

2. FORMULATION OF THE PROBLEM

We use rectangular Cartesian coordinates and the referential description of motion to study dynamic plane strain thermomechanical deformations of a prismatic body of rectangular cross-section (cf. Fig. 1a). The deformations of the body are governed by the following balance laws of mass, linear momentum, moment of momentum and internal energy.

$$\rho J = \rho_0, \qquad J = \det \boldsymbol{F}, \tag{1}$$

$$\rho_0 \dot{\boldsymbol{v}} = \mathrm{Div}\, \boldsymbol{T}, \tag{2}$$

$$\boldsymbol{T}\boldsymbol{F}^{\mathrm{T}} = \boldsymbol{F}\boldsymbol{T}^{\mathrm{T}} \tag{3}$$

$$\rho_0 \dot{e} = -\mathrm{Div}\boldsymbol{Q} + \mathrm{tr}(\boldsymbol{T}\dot{\boldsymbol{F}}^{\mathrm{T}}), \tag{4}$$

where $\boldsymbol{F}$ is the deformation gradient, ρ the present mass density of a material particle whose mass density in the stress-free reference configuration is ρ_0, $\boldsymbol{v}$ the present velocity of a material particle, $\boldsymbol{T}$ the first Piola–Kirchhoff stress tensor, e the specific internal energy, $\boldsymbol{Q}$ the heat flux measured per unit area in the reference configuration, Div the divergence operator with respect to coordinates in the reference configuration, and a superimposed dot indicates the material time derivative. In Eqn (4) we have assumed that all of the plastic working, rather than 90–95%, as asserted by Farren and Taylor [10] and Sulijoadikusumo and Dillon [11], is converted into heating.

We assume that the material is isotropic and can be modeled by the following constitutive relations.

$$\boldsymbol{\sigma} = -p\mathbf{1} + \boldsymbol{s}, \qquad p = K(\rho/\rho_0 - 1), \qquad \boldsymbol{\sigma} = J^{-1}\boldsymbol{T}\boldsymbol{F}^{\mathrm{T}}, \tag{5}$$

$$\dot{\boldsymbol{\sigma}} = \overset{\nabla}{\boldsymbol{\sigma}} + \boldsymbol{\sigma}\boldsymbol{W}^{\mathrm{T}} - \boldsymbol{W}\boldsymbol{\sigma}, \qquad \boldsymbol{W} = ((\mathrm{grad}\boldsymbol{v}) - (\mathrm{grad}\boldsymbol{v})^{\mathrm{T}})/2, \tag{6}$$

$$\overset{\nabla}{\boldsymbol{s}} = 2\mu(\bar{\boldsymbol{D}} - \bar{\boldsymbol{D}}^{\mathrm{p}}), \qquad \mathrm{tr}\,\boldsymbol{D}^{\mathrm{p}} = 0, \qquad \bar{\boldsymbol{D}} = \boldsymbol{D} - \left(\frac{1}{3}\mathrm{tr}\,\boldsymbol{D}\right)\mathbf{1}, \tag{7}$$

$$\dot{e} = c\dot{\theta} - p(\dot{\rho}/\rho^2), \qquad \boldsymbol{D} = ((\mathrm{grad}\boldsymbol{v}) + (\mathrm{grad}\boldsymbol{v})^{\mathrm{T}})/2, \tag{8}$$

$$\boldsymbol{q} = -k\,\mathrm{grad}\theta, \qquad \boldsymbol{q} = J^{-1}\boldsymbol{Q}\boldsymbol{F}^{\mathrm{T}}. \tag{9}$$

Here K is the bulk modulus, μ the shear modulus, c the specific heat, $\boldsymbol{W}$ the spin tensor, s the deviatoric Cauchy stress tensor, $\bar{\boldsymbol{D}}$ the deviatoric strain-rate tensor, and $\overset{\nabla}{\boldsymbol{\sigma}}$ is the Jaumann derivative of $\boldsymbol{\sigma}$. Equation $(7)_1$ is the deviatoric part of Hooke's law written in

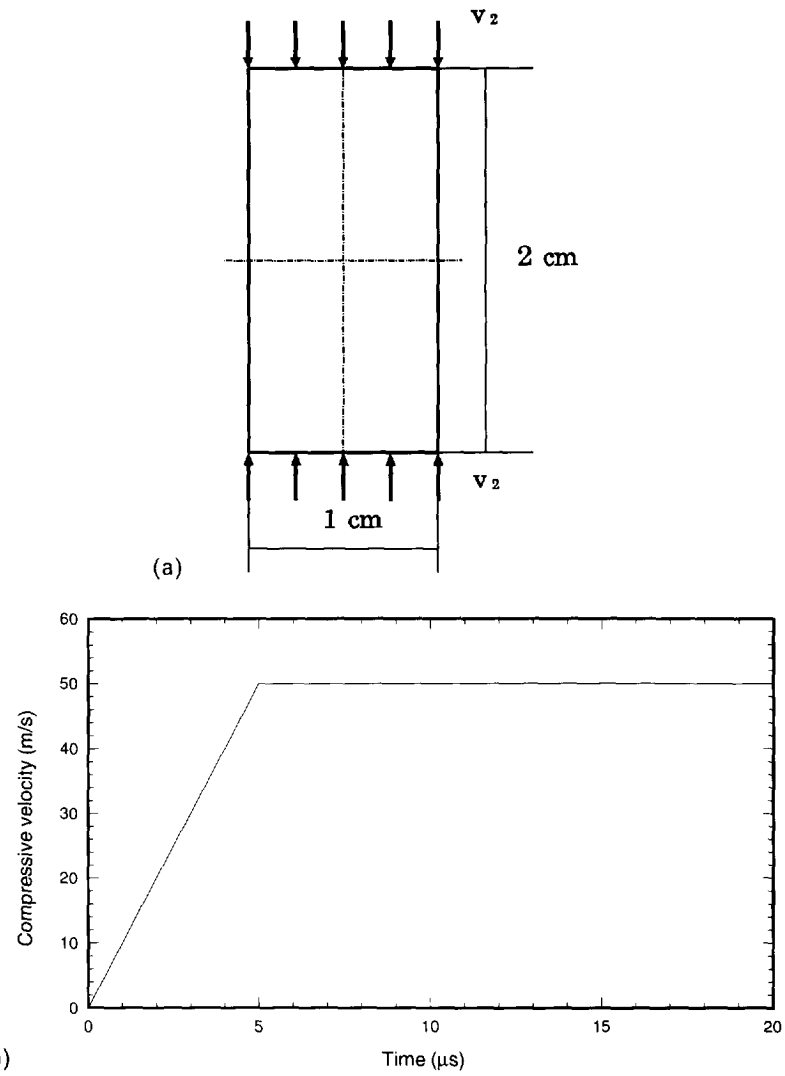

Fig. 1. A schematic sketch of the problem studied, and the time-dependence of the vertical component of velocity prescribed on the top surface.

the rate form. The deviatoric part $\bar{D}^p$ of the plastic strain-rate tensor is assumed to be given by

$$\bar{D}^p = \Lambda s. \tag{10}$$

Equation (10) implies that the plastic strain-rate is in the same direction as the deviatoric Cauchy stress s provided that $\Lambda > 0$. With

$$J_2 = \left(\frac{3}{2} s_{ij} s_{ij}\right)^{1/2}, \tag{11}$$

$$\Lambda = 0 \text{ if either } J_2 < \sigma_m, \text{ or } J_2 = \sigma_m \text{ and } s_{ij} D_{ij}^p \leqslant 0, \text{ and}$$

$$\Lambda > 0 \text{ if } J_2 > \sigma_m, \text{ or } J_2 = \sigma_m, \text{ and } s_{ij} D_{ij}^p > 0,$$

in which case it is a solution of the non-linear equation

$$J_2 = \sigma_m,$$

$$\sigma_m = (A + B(\varepsilon_p)^n)(1 + C \ln(\dot{\varepsilon}_p/\dot{\varepsilon}_0))(1 - T^m), \tag{12a}$$

$$\dot{\varepsilon}_p=\left(\frac{2}{3}\mathrm{tr}(\bar{\boldsymbol{D}}^p\bar{\boldsymbol{D}}^p\right)^{1/2}, \qquad \varepsilon_p=\int\dot{\varepsilon}_p\,dt, \qquad T=\frac{\theta-\theta_0}{\theta_m-\theta_0}. \tag{12b}$$

Equation $(12a)_2$ was proposed by Johnson and Cook [4] based upon the tests of thin tubular specimens conducted at moderate strain rates and temperatures. However, the range of temperatures and strain rates studied by them is not close to that likely to occur in a shear band problem. In Eqn (12) $\dot{\varepsilon}_p$ equals the effective plastic strain rate, $\dot{\varepsilon}_0$ is the reference strain-rate of $1\ s^{-1}$, ε_p the effective plastic strain, σ_m the effective flow stress, θ_0 the room temperature, θ_m the melting temperature of the material, and A, B, n, C and m are material constants.

For the initial conditions we take

$$\boldsymbol{\sigma}(\boldsymbol{X},0)=\boldsymbol{0} \qquad \rho(\boldsymbol{X},0)=\rho_0, \qquad \boldsymbol{v}(\boldsymbol{X},0)=\boldsymbol{0}, \qquad \theta(\boldsymbol{X},0)=\theta_0. \tag{13}$$

That is, the body is initially stress free, has uniform mass density ρ_0, is at rest and the initial temperature equals the room temperature θ_0. However, because of the presence of randomly distributed weak elements, the body is not homogeneous in the reference configuration. The body is loaded by prescribing the vertical component of velocity on the top and bottom surfaces. Because of the symmetry of initial and boundary conditions about the horizontal and vertical centroidal axes, we assume that its deformations at all times are symmetrical about these two centroidal axes and analyse deformations of only a quarter of the domain lying in the first quadrant. The pertinent boundary conditions are taken to be

$$\begin{gathered}
v_2(X_1,H,t)=\begin{cases}-v_0t/t_r, & 0\leqslant t\leqslant t_r,\\ -v_0, & t\geqslant t_r,\end{cases}\\
T_{12}(X_1,H,t)=0,\\
v_2(X_1,0,t)=0, \qquad T_{12}(X_1,0,t)=0,\\
T_{i1}(\hat{B},X_2,t)=0,\\
T_{21}(0,X_2,t)=0, \qquad v_1(0,X_2,t)=0,\\
Q_2(X_1,H,t)=Q_2(X_1,0,t)=Q_1(0,X_2,t)=Q_1(\hat{B},X_2,t)=0.
\end{gathered} \tag{14}$$

Here (X_1, X_2) denote coordinates of a material point in the reference configuration, t is the time, $2H$ is the height of the block, $2\hat{B}$ equals its width, and t_r equals the rise time for the prescribed velocity to increase from 0 to the steady value v_0; the load curve $(14)_1$ is depicted in Fig. 1b. Boundary conditions (14) imply that the bounding surfaces are thermally insulated, there are no tangential tractions on the top surface, bottom surface and the left vertical surface, and the right vertical surface is traction free.

3. COMPUTATION AND DISCUSSION OF RESULTS

In order to compute numerical results, we assigned the following values to various material and geometric parameters.

$$2\hat{B}=H=1\ \mathrm{cm}, \qquad v_0=50\ \mathrm{m\,s^{-1}}, \qquad t_r=5\ \mu\mathrm{s}. \tag{15}$$

For depleted uranium,

$$\begin{gathered}
A=1079\ \mathrm{MPa}, \qquad B=1119.69\ \mathrm{MPa}, \qquad C=0.007, \qquad n=0.25 \qquad m=1.0,\\
k=28\ \mathrm{W\,m^{\circ}C^{-1}}, \qquad \rho=18\,600\ \mathrm{kg\,m^{-3}}, \qquad \theta_m=1200^{\circ}\mathrm{C}, \qquad K=92\ \mathrm{GPa},\\
\mu=58\ \mathrm{GPa}, \qquad c=117\ \mathrm{J\,kg^{\circ}C^{-1}};
\end{gathered} \tag{16}$$

and for tungsten,

$$A = 1505.79\ \text{MPa}, \quad B = 176.5\ \text{MPa}, \quad C = 0.016, \quad n = 0.12, \quad m = 1.0,$$
$$k = 75\ \text{W m}^{\circ}\text{C}^{-1}, \quad \rho = 17\,000\ \text{kg m}^{-3}, \quad \theta_m = 1450^{\circ}\text{C}, \quad K = 257\ \text{GPa}, \quad (17)$$
$$\mu = 133\ \text{GPa}, \quad c = 134\ \text{J kg}^{\circ}\text{C}^{-1}.$$

Values of material parameters in the Johnson–Cook model are taken from Rajendran's report [5]. Even though these values are based on test data at strain-rates and temperatures higher than those used earlier by Johnson and Cook [4], the maximum temperatures and strain rates involved are nowhere close to those likely to occur in a shear band. For large variations in the temperature, nearly all of the material parameters in Eqn (12) and the shear and bulk moduli may be temperature dependent (e.g. see Klepaczko *et al.* [12]). Since test data for uranium and tungsten for the range of values of strain, strain rate and temperature likely to occur within a shear band are not available in the open literature, the dependence of material parameters upon temperature cannot be delineated and the error introduced by assuming the material parameters to be constants cannot be ascertained. Figures 2a and 2b depict the stress–strain curves for the uranium and tungsten blocks as computed from Eqn (12) at different values of the initial temperature and nominal strain rate. In plotting these it is assumed that the temperature does not vary while the body is

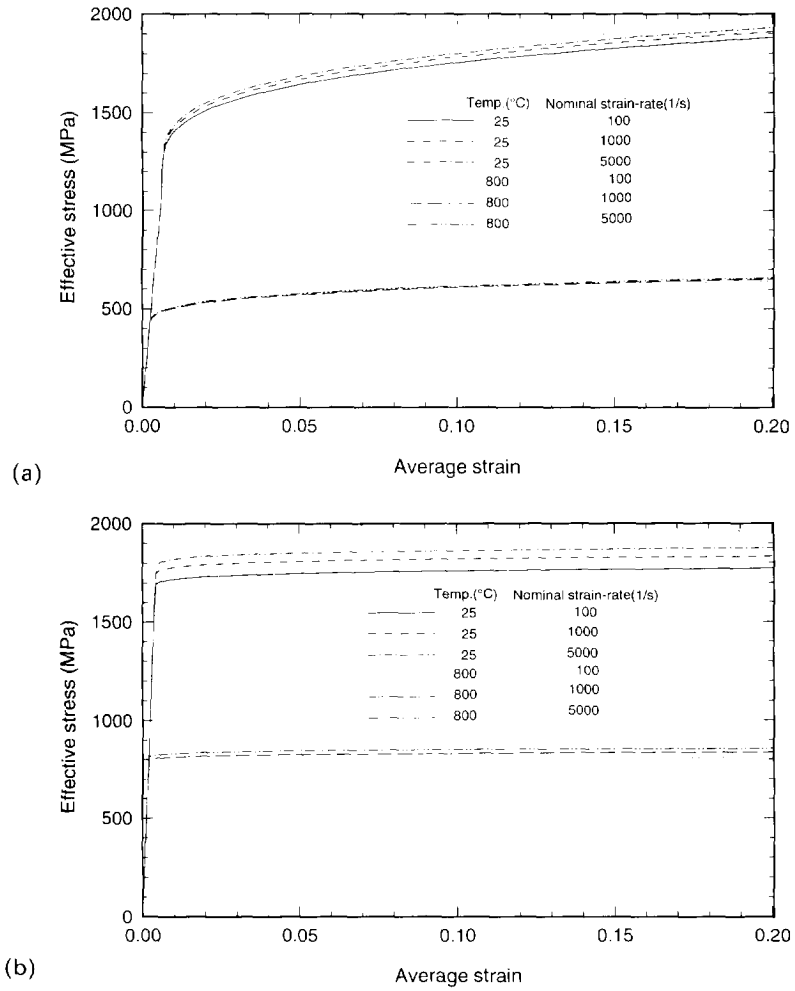

Fig. 2. Stress strain curves for (a) uranium and (b) tungsten at different strain rates and initial temperatures obtained from the Johnson Cook relation without solving an initial-boundary-value problem.

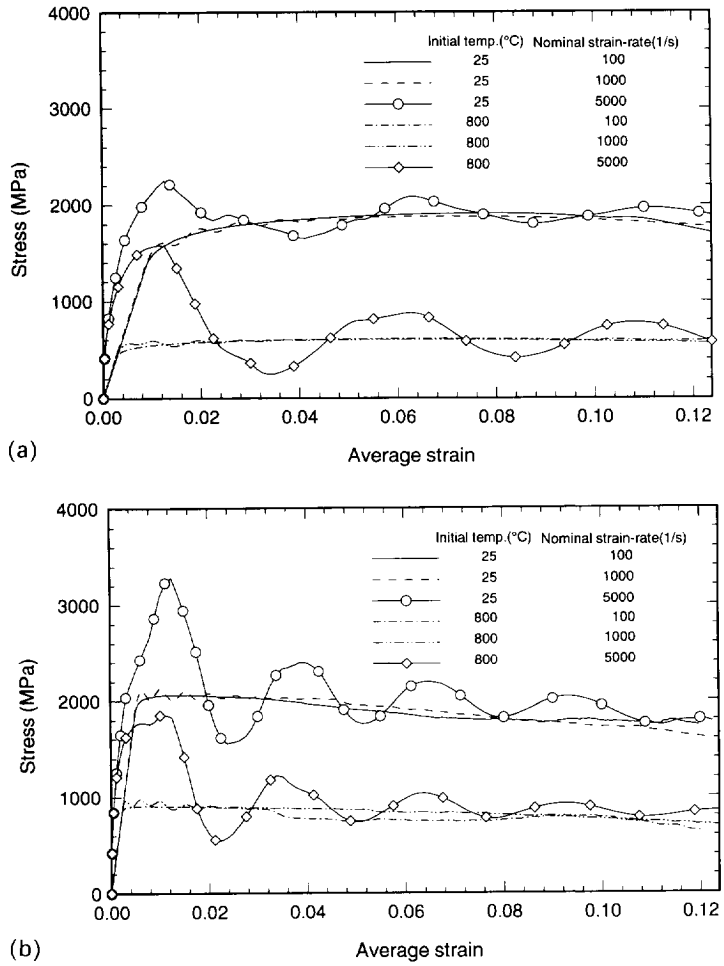

Fig. 3. Stress–strain curves for (a) uranium and (b) tungsten blocks deformed in plane strain compression at different nominal strain rates and initial temperatures; these curves are obtained by solving initial-boundary-value problems.

being deformed and no initial-boundary-value problem is solved. However, an experimentalist will observe the stress–strain curves shown in Figs 3a and 3b which are obtained by solving initial-boundary-value problems corresponding to plane strain deformations of a defect free homogeneous body. We note that the temperature continues to change and that the body may not deform homogeneously especially at the higher strain-rates considered. It is clear from these plots that uranium shows less strain-rate sensitivity than tungsten but exhibits a higher strain hardening effect.

For the prescribed value of v_0, the nominal strain rate increases from 0 to $5000\,s^{-1}$ in $5\,\mu s$, after which it remains steady. The problem is analysed by using a modified version of the large-scale explicit finite element code DYNA2D developed by Whirley *et al.* [13]. We have incorporated the effect of heat conduction into the code. It uses quadrilateral elements with one-point integration rule to evaluate various integrals and the hour-glass control to suppress the spurious modes. The time step is selected to satisfy the Courant condition. For a very fine mesh, the time step required to integrate satisfactorily the energy equation is considerably smaller than that needed for the momentum equation. In such cases, the energy equation should be integrated several times during one time step integration of the momentum equation. However, for the mesh used herein, the time step for the stable integration of the energy equation was larger than that for the integration of the momentum equation.

The domain, i.e. a quarter of the cross-section, in the reference configuration is divided into 10^4 uniform rectangular elements with 100 elements along the horizontal axis. It is

assumed that of these, randomly distributed 100, 200 or 300 elements are weak in the sense that, for them, values of A and B equal 95% of the values given in (16) and (17); the locations in the reference configuration of these weak elements are shown in Fig. 4. The presumed symmetry of deformations about the two centroidal axes necessitates that defects also be distributed symmetrically about the two centroidal axes.

Figures 5a and 5b depict respectively the deformed meshes for uranium and tungsten blocks at an average strain of 0.28 and 0.20 when there are 300 randomly distributed weak elements in the reference configuration; the results for 100 and 200 randomly distributed weak elements were qualitatively similar and hence are not shown. It is clear that for the

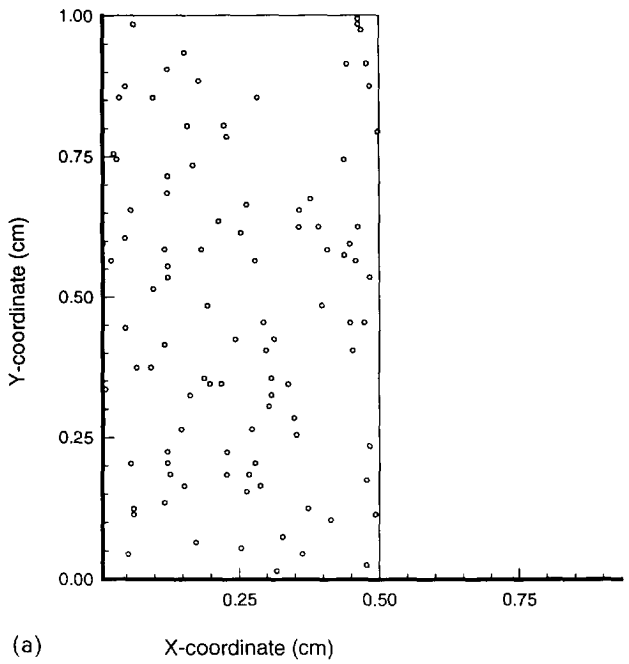

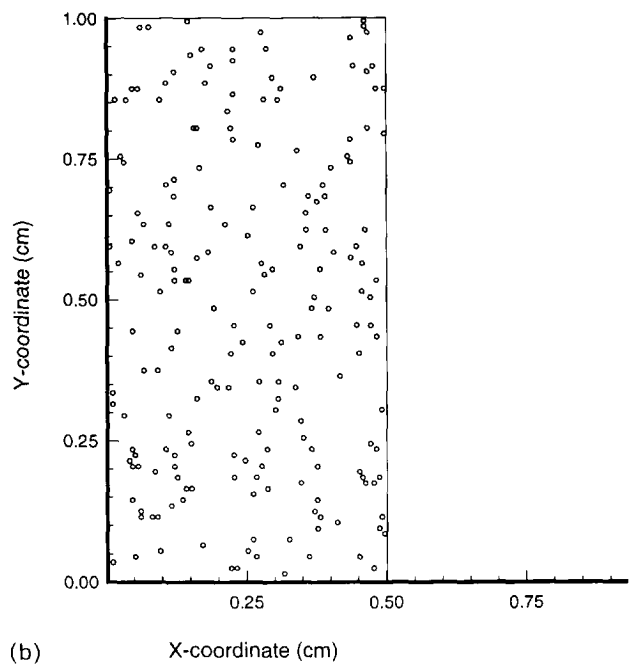

Fig. 4. *Continued*

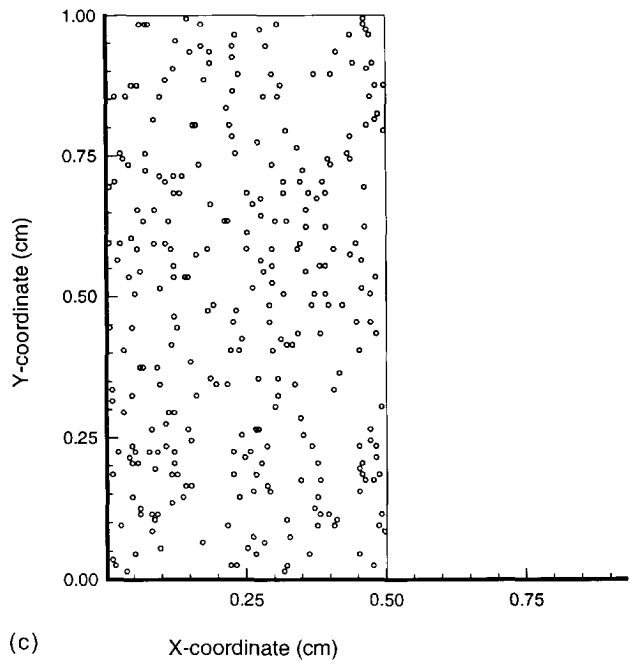

Fig. 4. Locations in the reference configuration of (a) 100, (b) 200 and (c) 300 randomly distributed weak elements.

uranium block, two shear bands each having a maximum effective plastic strain of 1.4, which is determined from the contours of the effective plastic strain, and at least two more in which the maximum effective plastic strain equals 0.56 have developed. Each one of these bands is inclined at an angle of approximately 42.5° counterclockwise with the horizontal; the slight deviation from the expected 45° direction could be due to the inhomogeneous deformations of the block and the band being not straight. The maximum temperature within the former two bands equals nearly 810°C and that in the latter two 360°C. There are also narrow regions of less intense plastic deformations that are nearly perpendicular to the four shear bands stated above. Since points on the left vertical edge are constrained from moving horizontally and those on the bottom surface from moving vertically, the only direction in which the material can expand is to the right. The deformations of the material enclosed by shear band boundaries are minuscule and it moves essentially as a rigid body resulting in striations on the right surface. Because of the randomly distributed defects, the deformations of the block are inherently non-homogeneous. The deformation patterns in the tungsten block, shown in Fig. 5b, are quite different from those in the uranium block. In the tungsten block, one dominant shear band as measured by the value of the maximum effective plastic strain in it forms at an angle of approximately 135° counterclockwise from the horizontal axis. This band is reflected from the left vertical edge into a weaker band inclined at an angle of nearly 45° counterclockwise with the horizontal axis. The maximum effective plastic strain in the dominant shear band equals 1.53, that in the reflected band equals 1.03, and in each of the other two weak bands parallel to the dominant one equals 0.54; the maximum temperature in each of these bands equals 815°C, 563°C, 311°C and 311°C, respectively. Thus the maximum temperature and the effective plastic strain in shear bands developed in uranium and tungsten blocks are nearly the same. We note that these occur at different values of the average strain or the non-dimensional time.

Since the effect of heat conduction is usually very small, especially when the time duration of the problem is of the order of tens of microseconds, according to the energy equation, the temperature rise at a point is essentially proportional to the total plastic work done there. This was confirmed by the plotted results too, since the contours of the temperature and effective plastic strain were identical. An examination of the contours of temperature rise in uranium and tungsten blocks at different times revealed the following. In the uranium

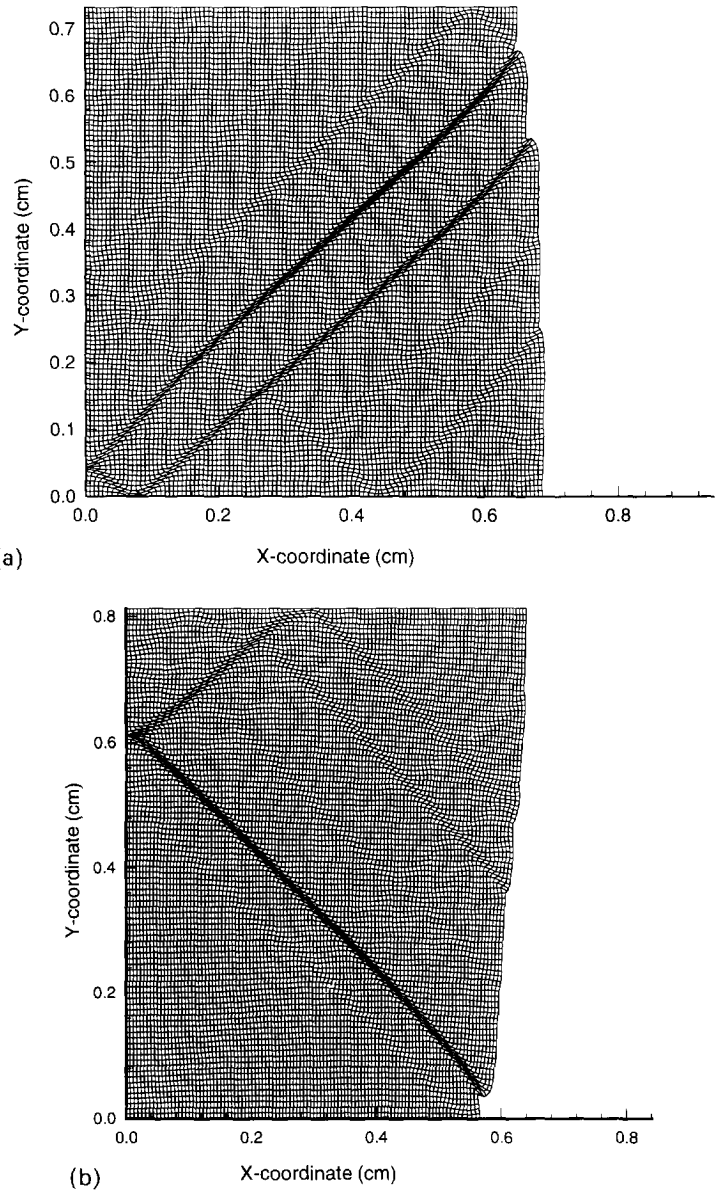

Fig. 5. Deformed meshes for the case of 300 randomly distributed weak elements: (a) for uranium block at an average strain of 0.28, and (b) for tungsten block at an average strain of 0.2.

block the temperature rise at an average strain of 0.1375 is higher in a rather large region near the centroid of the cross-section and also in a tiny region that adjoins the right boundary surface and is below the top right corner. The temperature rise and hence plastic deformations of the material in the top left portion and the bottom right region are nearly one-half of that of the material in the bottom left region. At an average strain of 0.1875, a kink in the right bounding surface and a little bit below the top right corner appears, and the temperature rise of the material aligned around the diagonal is 259°C, whereas that of the material in the bottom right portion is 169°C, and that of the material near the top left corner is below 169°C. At this time there are several thin parallel regions with temperature equal to 259°C. During subsequent compression of the uranium block several kinks form on the right bounding surface. Narrow regions of large plastic deformations, as also signified by the higher temperature, develop and adjoin these kinks. At an average strain of 0.2275, there are five such narrow regions, three of them with more intense plastic deformations than the other two. However, during continued compression of the block,

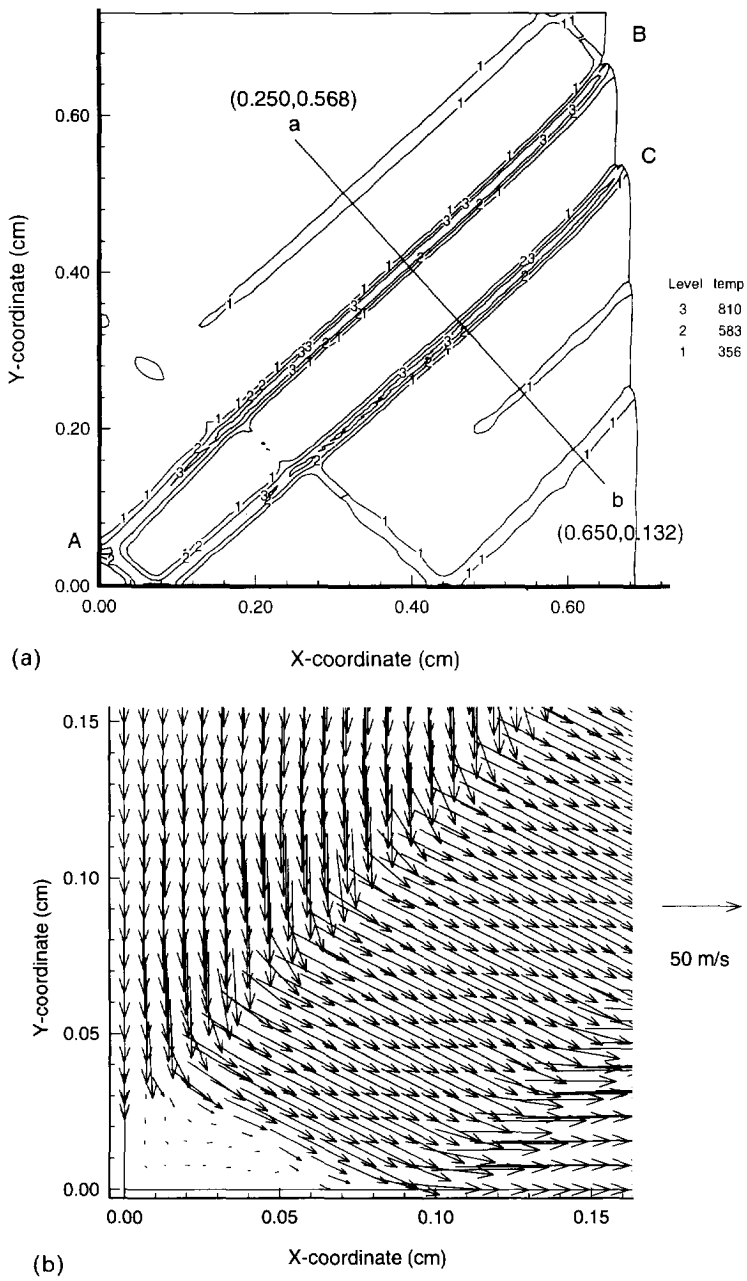

Fig. 6. *Continued*

plastic deformations in only two of these regions intensifies and steps in the right bounding surface appear. For the tungsten block, at an average strain of 0.0875, the material in the region near the top left corner is heated up more than that elsewhere. However, there is no clear delineation of regions of highest temperature. We should add that the deformations of the block are non-homogeneous because of the presence of weak elements. At an average strain of 0.1125, the initially vertical right edge gets inclined inwards near the bottom right corner, and at an average strain of 0.1275, a perceptible kink appears there. Note that for the uranium block a kink first appeared on the right boundary near the top right corner. At an average strain of 0.1375, a narrow region inclined at about 135° counterclockwise from the horizontal axis and abutting the kink develops. Subsequently more kinks form on the right bounding surface and parallel narrow regions of high temperature develop that adjoin these kinks. However, eventually only one dominant band passing through the

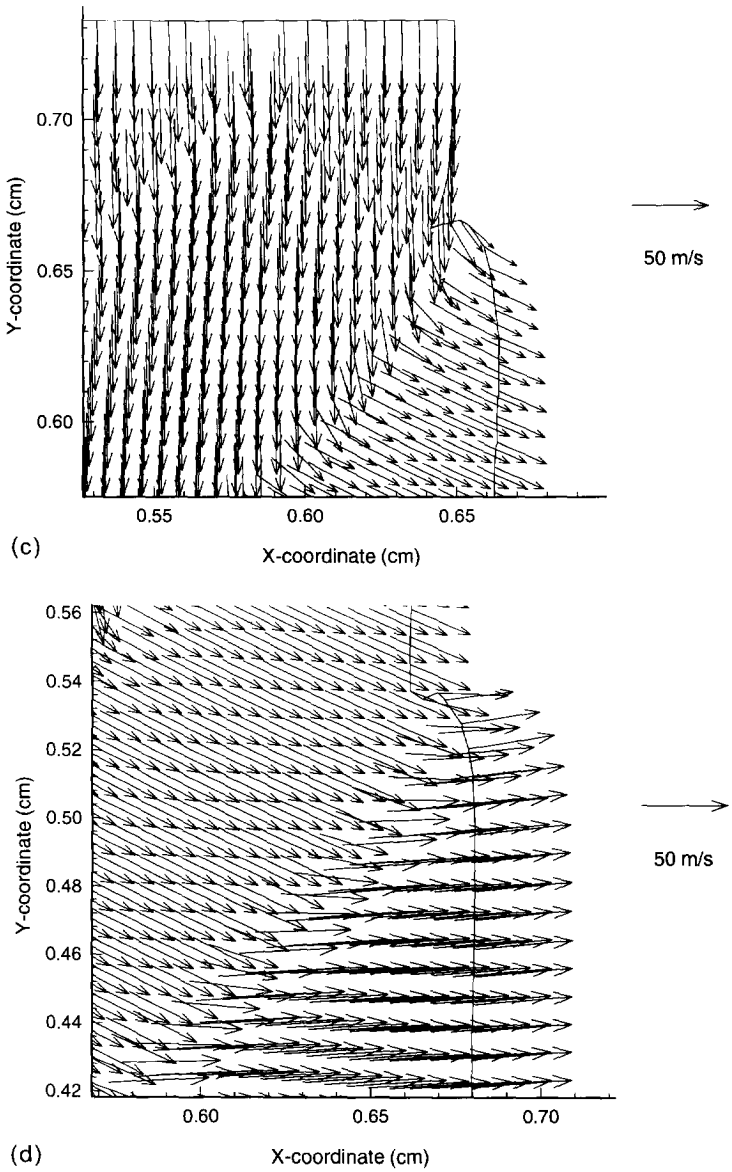

Fig. 6. (a) Locatons of points *A*, *B* and *C*, and the distribution of velocity field in the neighborhood of points (b) *A*, (c) *B* and (d) *C* in the deforming uranium block at an average strain of 0.2675.

clearly discernible discontinuity near the bottom of the right bounding surface develops. Why a kink first appears on the right bounding surface near the top right corner in uranium and the bottom right corner in tungsten is not clear. We will discuss below one possible reason for this difference.

Figure 6 shows the distribution of the velocity field in the deforming uranium block at an average strain of 0.2675 and in the neighborhood of three points A, B and C; the location of these points is shown in Fig. 7a. A close examination of the velocity field suggests that the deforming region is divided into four parts; the region above the upper 42.5° band is moving vertically down as a rigid body, and that in between the two 42.5° bands is moving as a rigid body but material particles have both horizontal and vertical components of velocity. The material region enclosed by the lower 42.5° band, the horizontal centroidal axis and the right bounding surface is moving as a rigid body to the right and that near the centroid of the cross-section is essentially at rest. Thus the velocity field changes in direction and/or magnitude across a shear band. Since the normal component of velocity

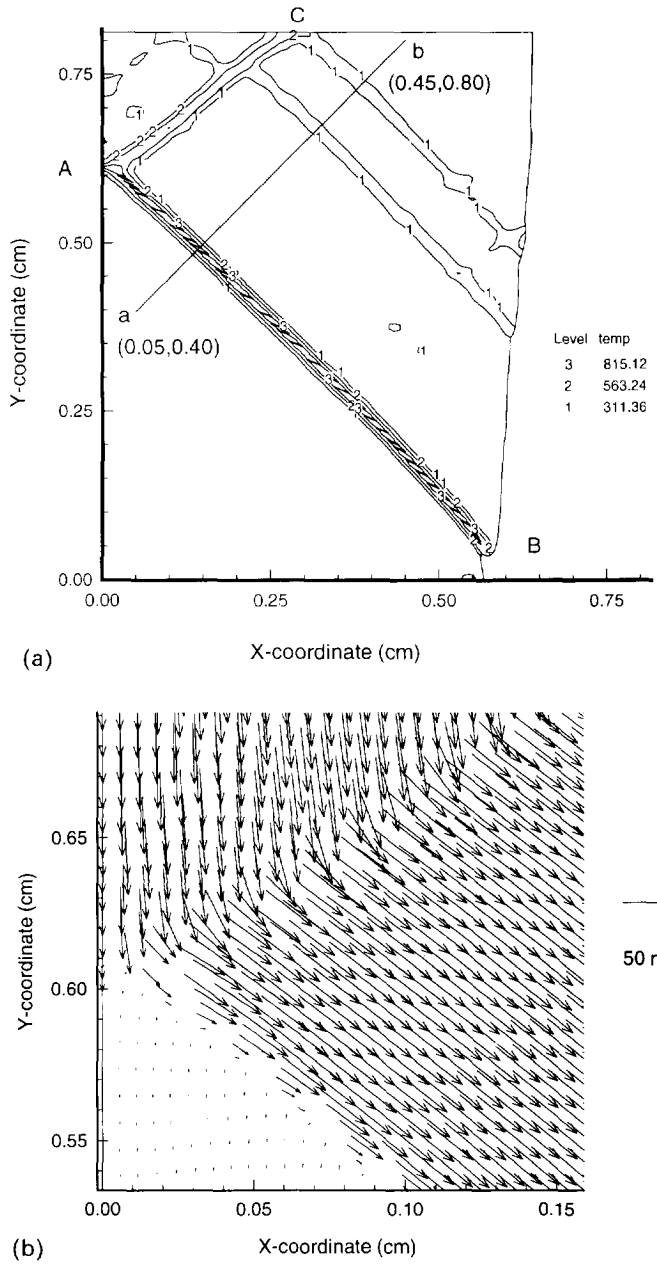

Fig. 7. *Continued*

across a shear band must be continuous, it is the tangential component that is discontinous as asserted by Tresca [14]. The velocity field in the neighborhood of points A, B and C in the deforming tungsten block at an average strain of 0.1875 is shown in Fig. 7. The dead zone, identified as the region whose material particles have practically zero speed, forms below the 135° band. The small region above the 45° band and enclosed by the vertical centroidal axis and the upper boundary is moving vertically downwards as a rigid body, and a rather large region enclosed by the 135° and 45° bands and the two bounding surfaces is deforming as a rigid body whose velocity has both horizontal and vertical components. The tangential component of the velocity field is discontinuous across the two shear bands.

In order to delineate the variation of the effective plastic strain and the effective plastic strain-rate within a shear band and at neighboring points, we have plotted in Figs 8 and 9 their distributions on the line *ab* perpendicular to the estimated centerline of the dominant

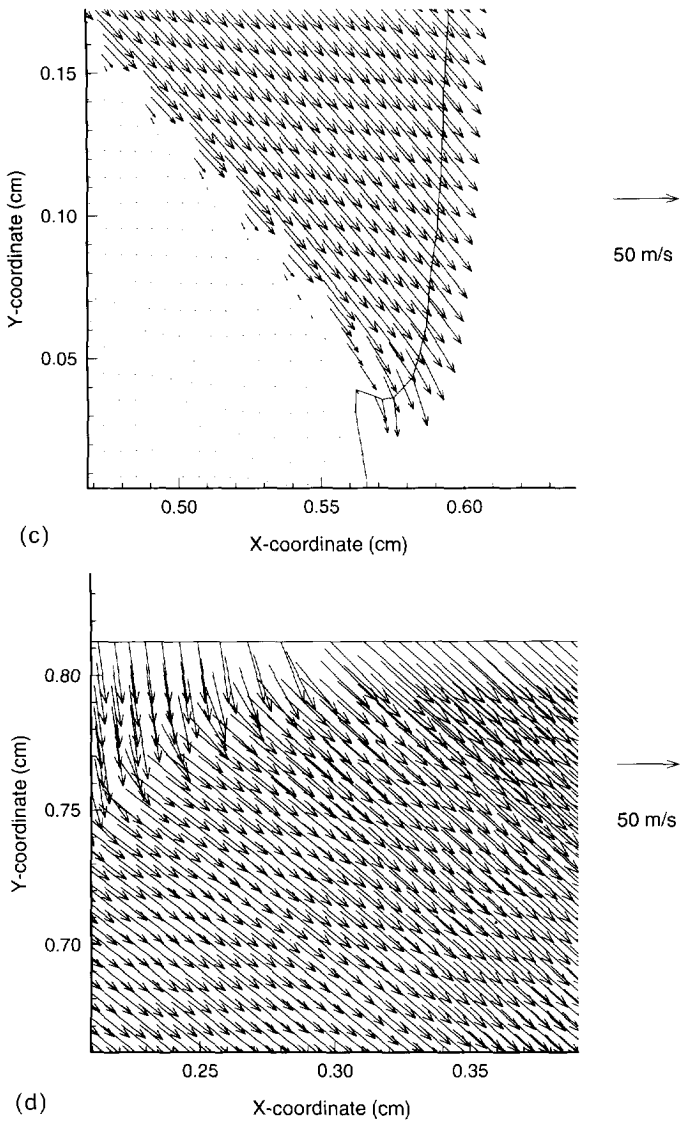

Fig. 7. (a) Locations of points A, B and C, and the distribution of the velocity field in the neighborhood of points (b) A, (c) B, and (d) C in the deforming tungsten block at an average strain of 0.1875.

band; the line ab is shown in Figs 6a and 7a, respectively, for the uranium and tungsten blocks. It is clear that the effective plastic strain and the effective plastic strain rate within the band is very high as compared with that at the neighboring points. The peak strain rate within the band is of the order of $10^5\ s^{-1}$ and far exceeds that used in the evaluation of material parameters. The width of the band(s) cannot be determined since the finite element mesh used is not fine enough. An optimum strategy will be to use an adaptively refined mesh as was done by Batra and Ko [15]. However, they used triangular elements. The finite element mesh used herein is the best we could use within the constraints of available computing resources.

In Fig. 10 we have plotted the time history of the compressive force required to deform uranium and tungsten blocks containing 0, 100, 200 and 300 randomly distributed weak elements with values of A and B equal to 95% of those given in (16) and (17). The abscissa, i.e. the average strain, equals the non-dimensional time. Marchand and Duffy [3] in torsion tests and Magness and Farrand [1] in compression tests characterized the initiation of shear bands as the instant when the load required to deform the specimen suddenly drops. With this criterion, shear bands initiate in tungsten at a lower value of the average strain

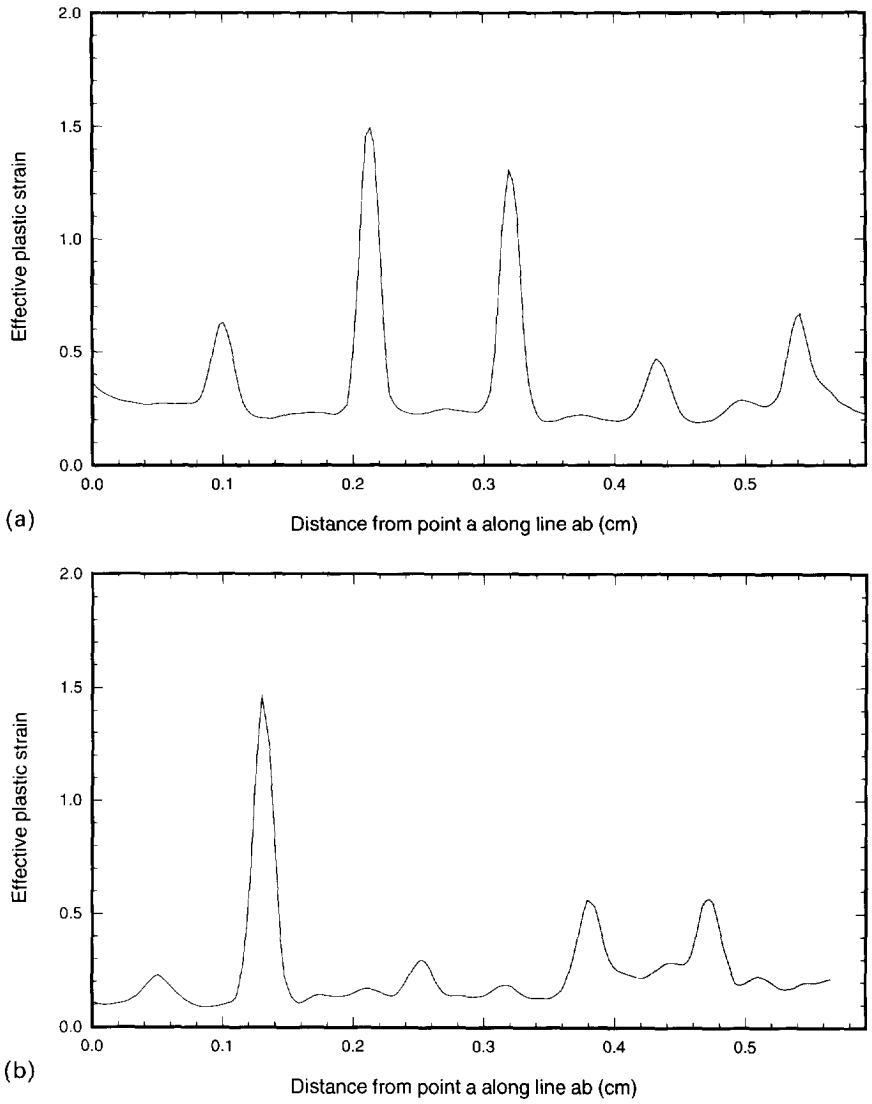

Fig. 8. Distribution of the effective plastic strain on a line perpendicular to the estimated centerline of the band for (a) the uranium block, and (b) the tungsten block.

than those in uranium. That damage can evolve even when there are no defects assumed to be present in the specimen has also been pointed out by Eftis *et al.* [16] in their numerical study of the microporous thermoviscoplastic materials deformed in tension. The oscillations in the load are due to inertial effects, and the higher amplitude and lower time period of oscillations for tungsten is due to the larger values of the shear and bulk moduli for it. The time period of oscillations is found to be the same as the time taken for an elastic wave to traverse a distance equal to twice the instantaneous height of the block. The load drops rapidly in uranium blocks but rather gradually in tungsten blocks. Both for uranium and tungsten blocks, an increase in the number of defects from 0 to 200 results in the load drop occurring at a lower value of the average strain, signifying that shear bands will initiate sooner with an increase in the number of defects. However, the average strain at which the load drops when there are 300 defects present is higher than that for the 200 defects, indicating that the shear bands need not always form sooner when the number of randomly distributed defects is increased.

The locations of 300 randomly distributed defects depend upon the seed numbers used to generate them. In addition to the case discussed above, we used three different sets of seed numbers to generate 300 random numbers. In each case, the orientations of shear

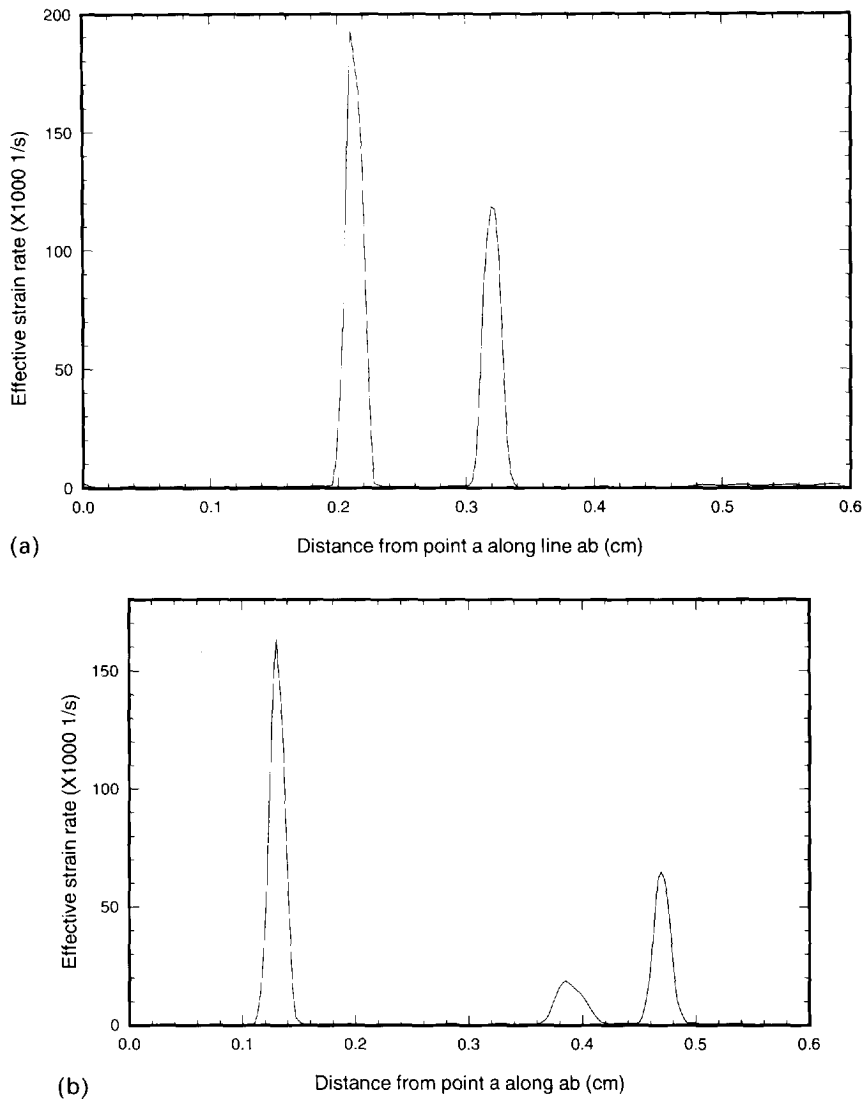

Fig. 9. Distribution of the effective plastic strain on a line perpendicular to the estimated centerline of the band for (a) the uranium block, and (b) the tungsten block.

bands in uranium and tungsten stayed essentially the same. However, the number of bands in the uranium block, their locations, and the values of the maximum effective plastic strain in them for the same value of the average strain were found to be different in each case. The vertical compressive load versus the average axial strain curves plotted in Fig. 11 reveal that, prior to the initiation of the shear band, the precise locations of randomly distributed defects do not affect in any noticeable way the load required to deform the block. However, they do influence the rate of load drop. The period of oscillations in the load for tungsten is less than that for uranium because of the higher values of the shear and bulk moduli for tungsten.

Since we are using a phenomenological theory and the specimen geometry and loading conditions are identical for tungsten and uranium blocks, the differences in the inclinations of shear bands in the two materials must be due to the difference in the values of material parameters. An examination of the values of material parameters given in (16) and (17) indicates that values of strain-hardening coefficient B, strain-hardening exponent n, strain-rate hardening coefficient C, thermal conductivity k, shear modulus μ and the bulk modulus K are noticeably different for the two materials. In order to see which one of these parameters affects the angle of inclination of the shear band, we artificially changed

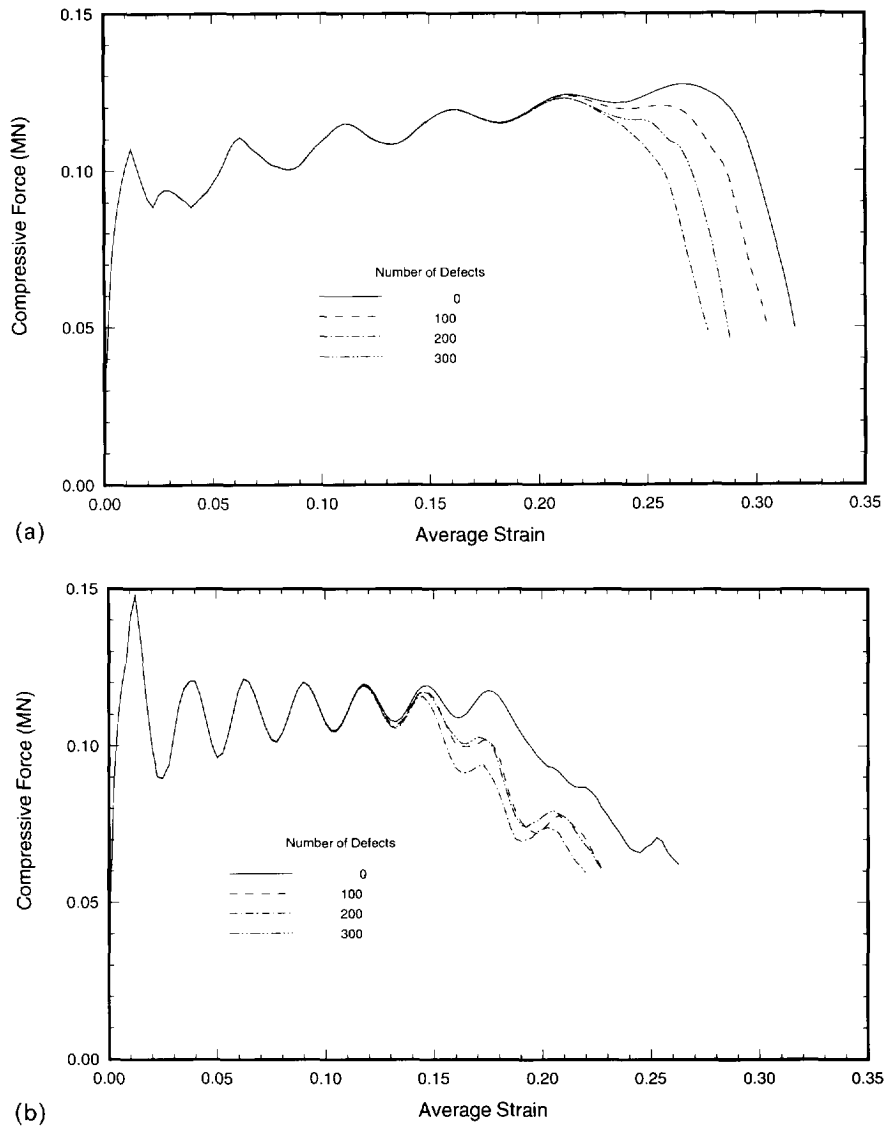

Fig. 10. Effect of number of randomly distributed defects on the compressive force required to deform the block vs the average strain (a) uranium block, and (b) tungsten block.

the value of one of these material parameters for tungsten to that for uranium and analysed the problem. These numerical experiments indicated that when the value of shear modulus for tungsten was changed from 133 GPa to 58 GPa so as to equal that for uranium, as depicted in Fig. 12a, the angle of inclination of the shear band was found to be nearly the same as that for uranium. For all other cases, the orientation of the band remained unchanged even though their number and locations varied. Figure 12b shows the deformed mesh for the fictitious tungsten block for which the value of bulk modulus K was reduced from 257 GPa to 92 GPa. It is clear that two parallel bands oriented essentially the same way as for the tungsten block (cf. Fig. 5b) formed. When the value of the strain-rate hardening coefficient C was lowered to that for uranium, several weak bands (i.e. the effective plastic strain in them was lower than that in shear bands formed in the original tungsten block) in addition to the two dominant ones were computed. However, the angle of inclination of the dominant bands was the same as that for the original tungsten material. This excercise suggests that the shear modulus strongly influences the angle of inclination of the shear band.

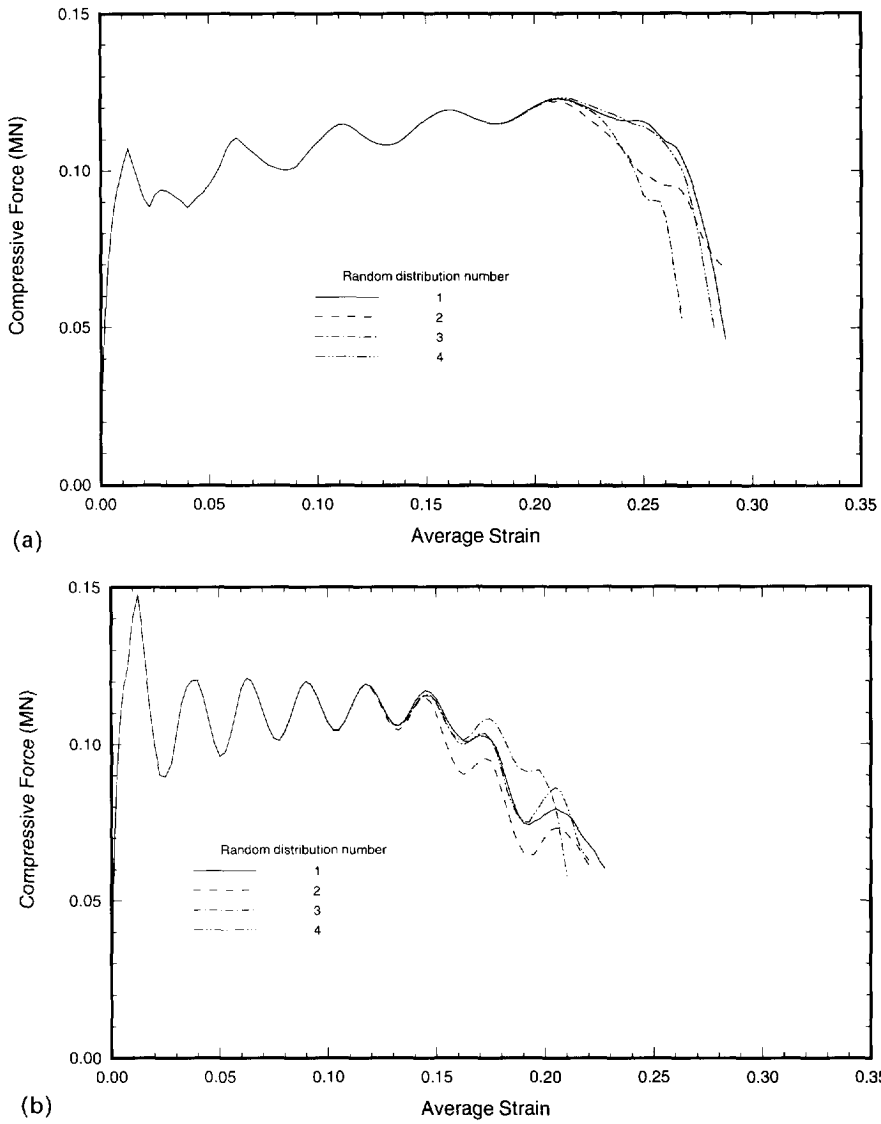

Fig. 11. Compressive force required to deform the block vs the average strain for four different random distributions of weak elements. (a) Uranium block and (b) tungsten block.

In order to assess the effect of the type of defects on the shear band formation, we varied the strength of defects by changing the values of A and B for them first from 95% of those given in (16) and (17) to 5% and then to 10^6 times of those given in (16) and (17). In the former case the defects are indeed very weak and can instantaneously deform plastically and in the latter case they simulate rigid inclusions. A scrutiny of the deformed meshes, not shown herein, revealed that the angles of inclination of the dominant shear bands were the same for defects modeled either as rigid inclusions or as 5% weak elements. However, when the defects were modeled as 95% weak elements, the bands in uranium and tungsten blocks were aligned in the same direction. Also, the type of defects influenced the locations of the bands. Figure 13 shows the time-history of the compressive load required to deform the uranium and tungsten blocks. The average strain at which shear bands form in uranium and tungsten was found to be lowest for 95% weak elements and maximum when the defects were modeled as 5% weak elements.

In order to assess the effect of heat conduction on the initiation of a shear band, we have plotted in Fig. 14 the time-history of the compressive force required to compress the block both with and without the consideration of heat conduction. It is clear that for

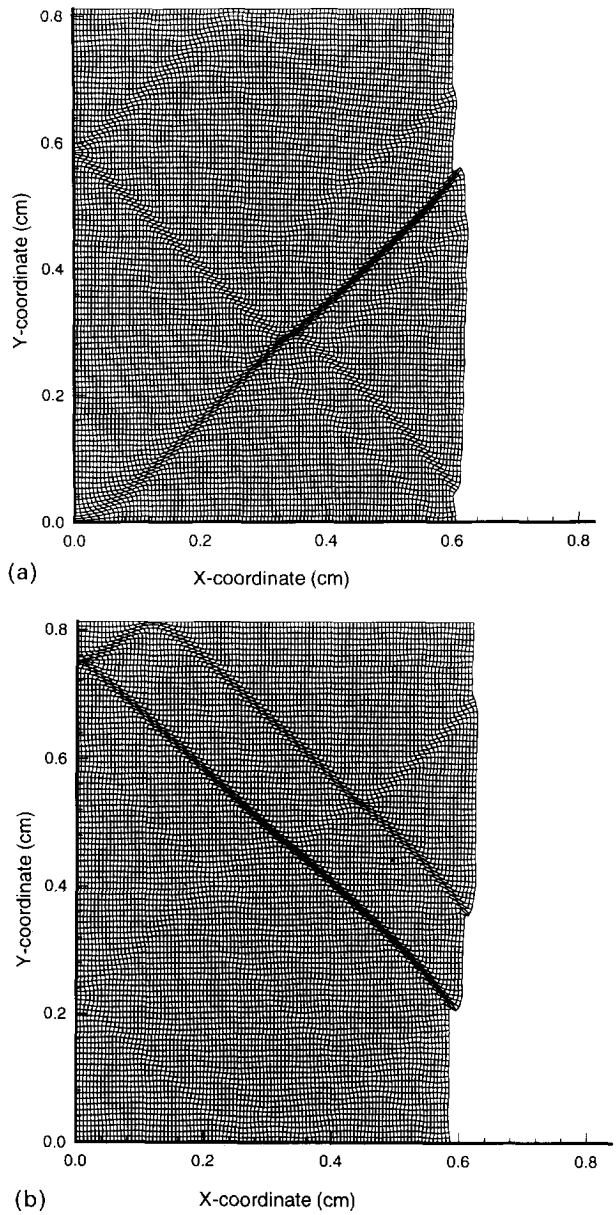

Fig. 12. Deformed meshes for the tungsten block when the value of (a) shear modulus was changed from 133 GPa to 58 GPa, (b) bulk modulus was changed from 257 GPa to 92 GPa.

uranium as well as tungsten, heat conduction affects minimally the value of the average strain at which a shear band initiates in them. Subsequent to the initiation of a shear band, the load drop is slightly lower when heat conduction effects are considered than that when they are neglected. We note that the values of non-dimensional thermal conductivity $k/\rho_c\theta_0$ for uranium and tungsten are quite low. Similar results were computed by Batra and Kim [17] who studied one-dimensional simple shearing deformations of a thermoviscoplastic body. We note that the angles of inclination of shear bands in uranium and tungsten blocks were not affected by the consideration of heat conduction.

CONCLUSIONS

We have studied the development of shear bands in plane strain compression of uranium and tungsten blocks deformed at a nominal strain-rate of $5000\,s^{-1}$. The rectangular

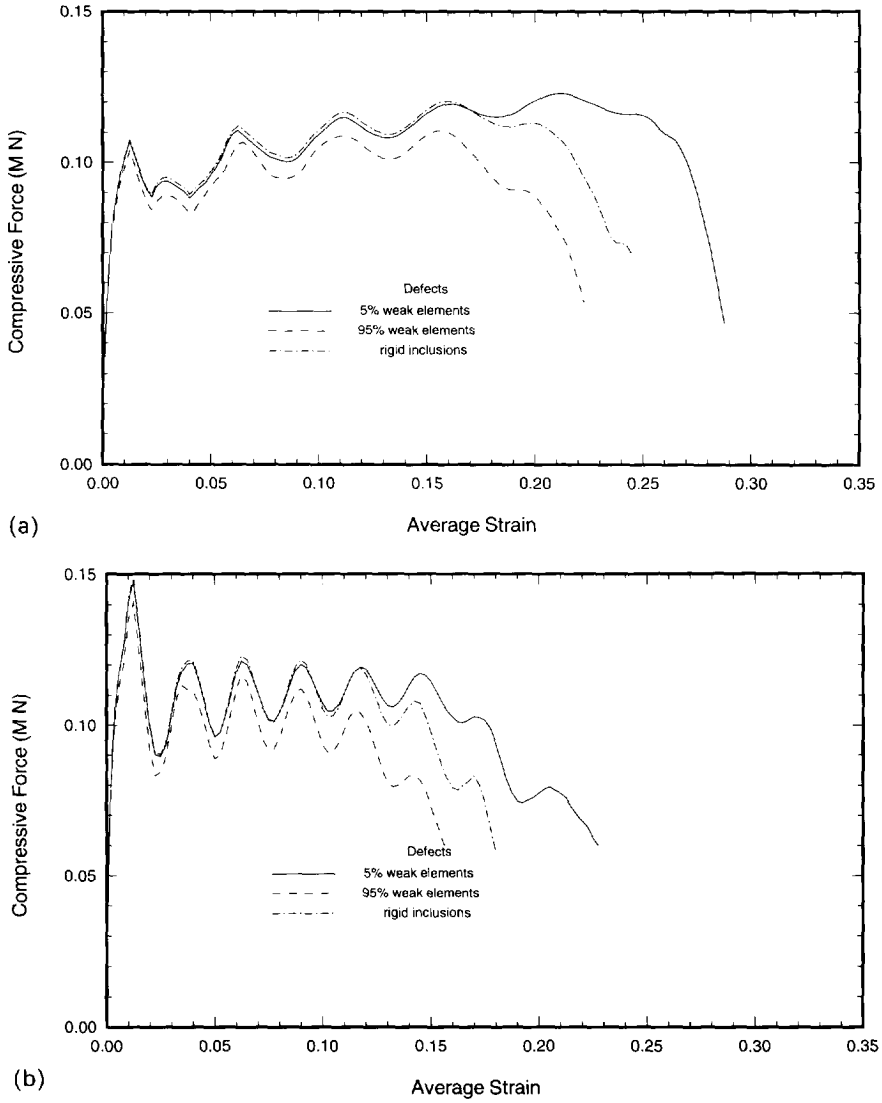

Fig. 13. The time-history of the load required to deform the blocks for different types of 300 randomly distributed defects; (a) uranium (b) tungsten.

cross-section of height to width ratio of 2 is assumed to have up to 300 randomly distributed weak elements for which the flow stress is taken to be 5% lower than that for the rest of the body. Four different random distributions of weak elements generated by using different seed data were examined. In each case more than one band formed, and the average strain at which a band initiated, as signified by the drop in the load required to deform the block varied a little. However, the load required to deform the block prior to the initiation of the shear band was found to be independent of the distribution of weak elements. The load drops more rapidly for uranium blocks as compared with that for tungsten blocks. Also, the average strain at which shear bands initiate in tungsten is lower than that in uranium. The size of the dead zone, defined as the material region whose particles are essentially at rest, is larger for the tungsten block than that for the uranium block. The dominant shear band, defined as the one with the maximum value of the effective plastic strain, was found to be inclined at 42.5° counterclockwise from the horizontal axis for uranium and 135° for tungsten. However, when either the shear modulus for the tungsten block was artificially changed to that for the uranium block, or the defects in both were modeled as 95% weak elements, the angle of inclination of the dominant shear band in

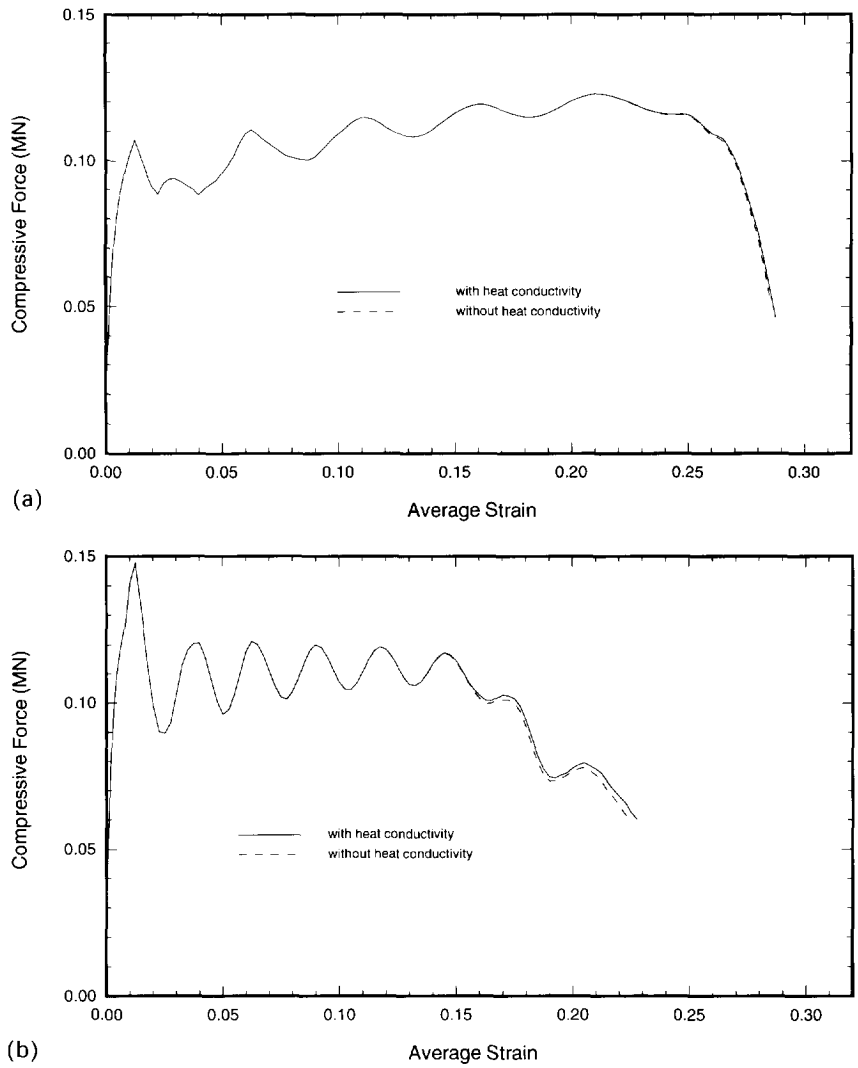

Fig. 14. Effect of heat conduction on the compressive force required to deform (a) the uranium and (b) the tungsten blocks. The insert illustrates the effect of heat conduction on the rate of load drop required to deform the blocks after the deformation has begun to localize.

each material was found to be approximately 42.5° counterclockwise from the horizontal axis.

Acknowledgements—This work was supported by the U.S. Army Research Office grants DAAL03-92-G-0315 to the University of Missouri-Rolla and DAAH04-95-1-0042 to the Virginia Polytechnic Institute and State University. Some of the computations were performed on the NSF supercomputer center at the Cornell University, Ithaca, NY. Z. Peng would like to thank Dr Yi Wu for discussions regarding the structure of the DYNA2D code which helped him incorporate the effects of heat conduction into the code.

REFERENCES

1. L. S. Magness and T. Farrand, Deformation behavior and its relationship to the penetration performance of high-density KE penetrator materials. *Proc. Army Science Conf.*, West Point, NY (1990).
2. R. C. Batra, X. T. Zhang and T. W. Wright, Critical strain ranking of twelve materials in deformations involving adiabatic shear bands. *J. Appl. Mech.* (in press).
3. A. Marchand and J. Duffy, An experimental study of the formation process of adiabatic shear bands in a structural steel. *J. Mech. Phys. Solids* **36**, 251–283 (1988).
4. G. R. Johnson and W. H. Cook, A constitutive model and data for metals subjected to large strains, high strain rates, and high temperatures. *Proc. 7th Int. Symp. Ballistics*, The Hague, The Netherlands, pp. 541–548 (1983).

5. A. M. Rajendran, High strain rate behavior of metals, ceramics, and concrete. Report No. WL-TR-92-4006, Wright Patterson Air Force Base (1992).
6. M. E. Backmann and S. A. Finnegan, The propagation of adiabatic shear. In *Metallurgical Effects at High Strain Rates*, pp. 531–543 (Edited by R. W. Rohde, B. M. Butcher, J. R. Holland and C. H. Karnes). Plenum Press, New York (1973).
7. H. M. Zbib, T. Shawki and R. C. Batra (Eds), *Material Instabilities*, Special Issue of *Appl. Mech. Rev.* **45**, No. 3, March (1992).
8. R. Armstrong, R. C. Batra, M. A. Meyers and T. W. Wright (Guest Editors), *Special Issue on Shear Instabilities and Viscoplasticity Theories, Mech. Mater.* **17**, 83–327 (1994).
9. G. R. Johnson, J. M. Hoegfeldt, U. S. Lindholm and A. Nagy, Response of various metals to large torsional strains over a large range of strain rates, Part 1: Ductile Metals. *ASME J. Engng Mater. Tech.* **105**, 42–47 (1983).
10. W. S. Farren and G. I. Taylor, The heat developed during plastic extrusion of metal. *Proc. R. Soc.* **A207**, 422– (1925).
11. A. U. Sulijoadikusumo and O. W. Dillon Jr. Temperature distribution for steady axisymmetric extrusion with an application to Ti-6Al-4V, Part 1. *J. Thermal Stresses* **2**, 97–112 (1979).
12. J. R. Klepaczko, P. Lipinski and A. Molinari, An analysis of the thermoplastic catastrophic shear in some metals. *Proc. Int. Conf. on Impact Loading and Dynamic Behavior of Materials*, pp. 695–704 (Edited by C. Y. Chiem *et al.*). Informations gesellaschaft Verlag Oberursel (1987).
13. R. G. Whirley, B. E. Englemann and J. P. Hallquist, DYNA2D, A Nonlinear, Explicit, Two-Dimensional Finite Element Code for Solid Mechanics, User Manual, Lawrence Livermore National Laboratory Report, UCRL-MA-110630 (1992).
14. H. F. Tresca, On further application of the flow of solids. *Proc. Inst. Mech. Engr.* **30**, 301–345 (1978).
15. R. C. Batra and K. I. Ko, An adaptive mesh refinement technique for the analysis of shear bands in plane strain compression of a thermoviscoplastic solid. *Comp. Mech.* **10**, 369–379 (1992).
16. J. Eftis, J. A. Nemes and P. W. Randles, Viscoplastic analysis of plate-impact spallation. *Int. J. Plasticity* **7**, 15–40 (1992).
17. R. C. Batra and C. H. Kim, Effect of thermal conductivity on the initiation, growth, and band width of adiabatic shear bands. *Int. J. Engng Sci.* **29**, 949–960 (1991).